Adaptive Cost Function-Based Shared Driving Control for Cooperative Lane-Keeping Systems With User-Test Experiments

Mohamed Radjeb Oudainia, Chouki Sentouh, Anh-Tu Nguyen, Jean-Christophe Popieul

Adaptive Cost Function-Based Shared Driving Control for Cooperative Lane-Keeping Systems With User-Test Experiments

Article *in* IEEE Transactions on Intelligent Vehicles · September 2023

DOI: 10.1109/TIV.2023.3317979

CITATIONS
0

READS
78

4 authors:

Mohamed Radjeb Oudainia
Université Polytechnique Hauts-de-France
5 PUBLICATIONS **7** CITATIONS
SEE PROFILE

Chouki Sentouh
LAMIH UMR CNRS 8201 Hauts-de-France Polytechnic University
114 PUBLICATIONS **2,071** CITATIONS
SEE PROFILE

Anh-Tu Nguyen
Université Polytechnique Hauts-de-France
140 PUBLICATIONS **2,106** CITATIONS
SEE PROFILE

J.-C. Popieul
Université Polytechnique Hauts-de-France
61 PUBLICATIONS **442** CITATIONS
SEE PROFILE

Adaptive Cost Function-Based Shared Driving Control for Cooperative Lane-Keeping Systems with User-Test Experiments

Mohamed Radjeb Oudainia, Chouki Sentouh, Anh-Tu Nguyen*, *Senior Member, IEEE*, Jean-Christophe Popieul

***Abstract*—This paper presents a new shared control method with a dynamic driver-automation conflict management for cooperative lane keeping systems (LKS) of automated vehicles. Based on a human-centered control approach, the proposed shared control design takes into account the driver's activity and availability, as well as the surrounding risk to *dynamically* adapt the driving assistance level via an adaptive cost function. To this end, we propose a method to characterize in real-time the driver's activity, which allows for an appropriate assistance level according to the driving conditions. Linear parameter-varying (LPV) control technique is leveraged to deal with the time-varying nature of the vehicle speed and the level of assistance. The uncertainties of the lateral tires forces are taken into account in the control design via a norm-bounded representation. Using Lyapunov stability theory, the control design conditions are derived in terms of linear matrix inequality (LMI) constraints, which can be effectively solved by semidefinite programming techniques. User-test experiments are performed with the SHERPA dynamic car simulator to demonstrate the effectiveness of the proposed shared control method from both objective and subjective viewpoints.**

***Index Terms*—Lane-keeping systems, cooperative control, human-in-the-loop control, human-machine interaction, shared control, automated driving.**

NOMENCLATURE

M_v	Mass of vehicle $[kg]$
I_z, J_s	Yaw and steer inertia $[kg.m^2]$
v_x	Longitudinal velocity $[m/s]$
β, δ_d	Sideslip angle, steering wheel angle $[rad]$
f_w	Crosswinds force $[N]$
ψ_L	Heading error $[rad]$
y_L	Lateral position error $[m]$
α_f, α_r	Front and rear slip angles $[rad]$
C_f, C_f	Front and rear cornering stiffness $[N/rad]$
r	Yaw rate $[rad/s]$
l_f, l_r	Distance from COG to front and rear axles $[m]$
T_s, T_d, T_a	Self-align, driver and automation torque $[N.m]$
R_s, B_s	Steer gear ratio, steering system damping

I. INTRODUCTION

In the field of automated vehicles, the notion of cooperation between the human driver and the automation system in advanced driver assistance systems (ADAS) has been received increasing attention from both academic and industrial researchers [1]–[4]. An ADAS system actively helps the driver to execute the driving task, such as lane keeping systems (LKS), or lane change systems (LCS). However, the interaction between the driver and the ADAS raises a number of questions about the transfer of authority and responsibility between them [5], [6]. The current challenge of ADAS developments is to incorporate the driver as an active operator in the vehicle control loop. In recent works, ADAS based on driver-in-the-loop designs have been used to solve a variety of human-machine interaction issues, including the sharing and transfer of authority [7]–[9], the conflict minimization [5], [10]–[12], and the reduction of the driver workload [13]–[15]. Despite technological advances, the development of control strategies that allow ADAS systems to share the driving responsibility and authority with the human driver still remains an open research question [6], [16].

A. Related Works

Shared control strategies taking into account the driver behaviors have been largely studied to improve the human-machine cooperation [6], [17]. Based on the driver's actions, a cooperative path planning algorithm was proposed in [18] to deal with the driver-automation conflict issue. A cooperative framework based on data-driven adaptive dynamic programming and a learning iteration model was developed in [19] to achieve desired steering performance. A driver-automation cooperation oriented approach was proposed in [5] for shared control between the human driver and the LKS system. Based on a weighting approach, Nguyen et *al.* [10] developed a shared steering controller, which is able to effectively manage the trade-off between the lane keeping performance and the negative system interference. An $\mathscr{H}_2/\mathscr{H}_\infty$ haptic shared control method was proposed in [9] to facilitate the transitions between manual and autonomous driving modes. However, these shared control methods require the information about the driver parameters, which cannot be obtained precisely for a large class of human drivers with various driving styles [20]. It is important to note that these existing works do not consider the driver inattention or hypovigilance in the shared control design. Ansari et *al.* [17] investigated the impact of different driving conditions as well as driver behaviors and errors on the vehicle control performance. To enhance the dependability and the safety of shared steering control systems, an extended system with an adaptive authority allocation model was proposed

The authors are with the Univ. Polytechnique Hauts-de-France, LAMIH, CNRS, UMR 8201, Valenciennes, France. C. Sentouh, A.-T. Nguyen, and J.-C. Popieul are also with the INSA Hauts-de-France, F-59313 Valenciennes, France (e-mail: firstname.lastname@uphf.fr).

This research has been done within the framework of the CoCoVeIA project (ANR-19-CE22-0009-01), funded by the Agence Nationale de la Recherche, the Ministry of Higher Education and Research and the French National Center for Scientific Research.

*Corresponding author: Anh-Tu Nguyen (nguyen.trananhtu@gmail.com).

in [21]. Using a model reference adaptive control algorithm, Wu et *al.* [22] proposed a method to adjust the steering torque based on the driver's behavior and the vehicle dynamics. Considering the vehicle handling dynamics and the driver's driving intention, a shared control method was developed in [23] based on an inverse vehicle dynamics model. An adaptive shared control approach was proposed in [24] to mitigate the risks associated with partial automation failures by enabling smooth and safe transitions between autonomous and manual driving modes. Based on a model predictive control (MPC) technique, a new shared steering controller was designed in [25] to dynamically optimize the driving authority allocation between the human driver and the autonomous system. An indirect shared control method for steer-by-wire vehicles was developed in [26], where the authors employed a weighted summation approach to balance the control inputs of the driver and the automation. Another indirect shared control method, designed under the framework of non-zero sum differential game, was proposed in [27]. A safe cooperative driving approach on curvy roads through coordinated longitudinal and lateral control strategies was introduced in [28]. A multi-constraints MPC shared controller was proposed in [29] to assist drivers in path tracking and collision avoidance, where driver-data-based performance indices are used to define the control authority for the steering assistance system. In [30], an adaptive steering torque coupling framework was proposed, where the shared steering system is modeled based on a non-cooperative dynamic game.

Despite great advances, the existing shared control approaches still face major challenges related to vehicle stability guarantee and allocation of driving responsibility [16]. Indeed, the well-known weighted summation method, used to distribute the control authority between the driver and the automation, has limitations in ensuring the overall stability of the human-machine vehicle system. Moreover, allocating the responsibility with human drivers under various driving scenarios remains a complex issue [6]. To overcome these challenges, we propose a new human-machine interaction strategy to allow for a gradual and continuous sharing of the vehicle control between the driver and the LKS system.

B. Proposed Methodology and Contributions

This paper investigates the human-centered concept for shared steering control design of a cooperative LKS system. Using the steering torque input as a control signal, we focus on minimizing the conflict when both the human driver and the LKS automation jointly perform driving tasks. The proposed adaptive human-machine shared control architecture is illustrated in Fig. 1. To effectively handle the driver-LKS conflict, we dynamically adjust the objective cost function used for shared control design. This adaptive cost function is defined using the real-time driving assistance level to appropriately assist the driver to perform the driving task. The assistance level is determined based on the online information related to the surrounding driving risks, as well as the driving availability and activity of the human driver. To deal with the time-varying nature of the vehicle speed and especially the driving assistance parameter, linear parameter-varying (LPV) control framework is leveraged together with Lyapunov stability theory to design a robust shared steering controller. A preliminary version of this work was presented in [31]. The new contributions can be summarized as follows.

- We propose a method to characterize the online driver's driving activity, depending his/her physical and mental workloads. Such a characterization is crucial to construct a multi-objective cost function for shared control design. Taking into account the real-time information on the availability and activity of the driver, and the traffic conditions, this adaptive cost function allows for an effective driver-LKS conflict management.
- A polytopic LPV control framework is used to take into account the dynamic variation of not only the vehicle speed but especially the driving assistance parameter, involved in the adaptive cost function. The design conditions are expressed in terms of LMI constraints, where the cost function can be minimized via a convex optimization.
- User-test experiments are performed with the SHERPA car simulator and human drivers to show the effectiveness of the proposed shared control method in terms of lane keeping performance, control robustness with respect to uncertainties/disturbances, human-machine conflict mitigation, and especially driver acceptability.

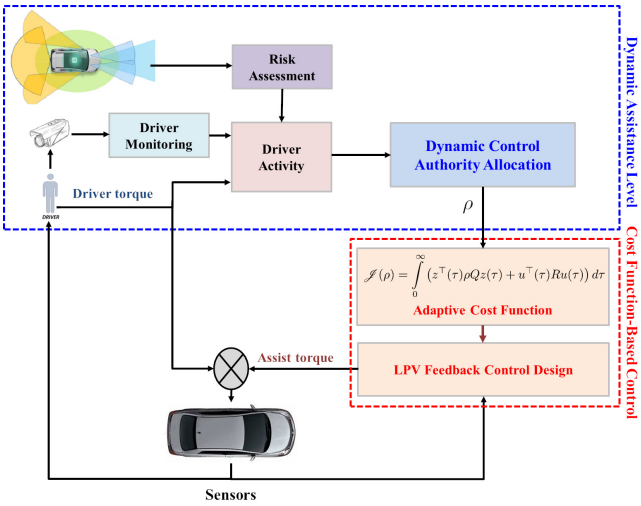

Fig. 1: Adaptive cost function-based shared control scheme.

Notations. $\mathbb{R}^{m\times n}$ denotes the set of $m \times n$ matrices with real elements. I is an identity matrix of appropriate dimensions. For a matrix X, $X^\top$ is the transpose of X, X^{-1} is its inverse, and $\mathrm{He}(X) = X + X^\top$. The expression $X \succ Y$ means that $X - Y$ is a positive definite matrix. For matrices Y_1 and Y_2, $\mathrm{diag}(Y_1, Y_2)$ stands for block diagonal matrix. The symbol $*$ stands for matrix blocks that can be deduced by symmetry. Let $\mathcal{L}_2[0, +\infty]$ be the set of bounded functions $f : \mathbb{R}^+ \to \mathbb{R}^m$ with respect to the norm $\|f\|_2 = \sqrt{\int_0^\infty f^\top(t) f(t) dt} < \infty$.

II. Vehicle Modeling

For shared driving control design, we consider a two degrees-of-freedom vehicle model depicted in Fig. 2. Under

standard driving conditions with small angles assumption and no longitudinal slip, the vehicle dynamics is described as [5]

$$\begin{aligned}\dot{\beta} &= -\frac{2\left(C_f + C_r\right)}{M_v v_x}\beta + \left(\frac{2\left(C_r l_r - C_f l_f\right)}{M_v v_x^2} - 1\right) r \\ &\quad + \frac{2C_f}{M_v v_x}\delta + \frac{1}{M_v v_x} f_w \\ \dot{r} &= \frac{2\left(C_r l_r - C_f l_f\right)}{I_z}\beta - \frac{2\left(C_r l_r^2 + C_f l_f^2\right)}{v_x I_z} r \\ &\quad + \frac{2C_f l_f}{I_z}\delta + \frac{l_w}{I_z} f_w\end{aligned} \tag{1}$$

where δ is the steering wheel angle. The dynamics of the lateral position error y_L, and the heading errors ψ_L at a look-ahead distance l_p can be represented by [5]

$$\begin{aligned}\dot{\psi}_L &= r - \rho_c v_x \\ \dot{y}_L &= \beta v_x + l_p r + \psi_L v_x\end{aligned} \tag{2}$$

where ρ_c is the road curvature. The dynamics of the steering column system is given by

$$J_s \ddot{\delta}_d = -B_s \dot{\delta}_d + T_c - T_s \tag{3}$$

where $T_c = T_a + T_d$ is the combined steering torque. The self-alignment torque T_s in (3) can be expressed as

$$T_s = \frac{-2C_f g_t}{R_s}\beta + \frac{-2l_f C_f g_t}{R_s v_x} r + \frac{2C_f g_t}{R_s^2}\delta$$

where g_t is the width of the tire contact.

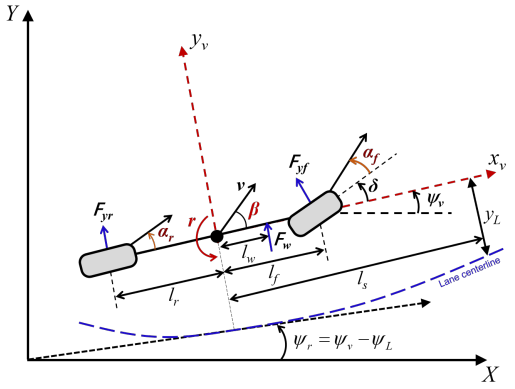

Fig. 2: Schematic of a two degrees-of-freedom vehicle model.

To take into account the properties of the road surfaces, *e.g.*, dry, wet or snowy roads, the following uncertain tires model is used to represent the tire-friction interaction [32]:

$$C_f = C_{f_0} + \Delta_f \zeta(t), \quad C_r = C_{r_0} + \Delta_r \zeta(t) \tag{4}$$

where $|\zeta(t)| \leq 1$, for $\forall t \geq 0$, is an unknown parameter, and

$$\begin{aligned}C_{f_0} &= \frac{1}{2}\left(\overline{C}_f + \underline{C}_f\right), \quad C_{r_0} = \frac{1}{2}\left(\overline{C}_r + \underline{C}_r\right) \\ \Delta_f &= \frac{1}{2}\left(\overline{C}_f - \underline{C}_f\right), \quad \Delta_r = \frac{1}{2}\left(\overline{C}_r - \underline{C}_r\right)\end{aligned}$$

The upper bounds and lower bounds of the front and rear cornering stiffness coefficients, *i.e.*, $C_f \in \left[\overline{C}_f, \underline{C}_f\right]$ and $C_r \in \left[\overline{C}_r, \underline{C}_r\right]$, can be determined by exploiting the relationship between slip angle and lateral tire forces for a class of road surfaces. Then, the road-vehicle system can be defined from (1), (2), (3) and (4), as

$$\dot{x} = (A(v_x) + \Delta A(v_x))x + Bu + E(v_x)d \tag{5}$$

where $x = \begin{bmatrix}\beta & r & \psi_L & y_L & \delta_d & \dot{\delta}_d\end{bmatrix}^\top$ is the vehicle state, $u = T_c$ is the vehicle control input, and $d = \begin{bmatrix}f_w & \rho_c\end{bmatrix}^\top$ is the disturbance vector. The state-space matrices of system (5) are defined by

$$A(v_x) = \begin{bmatrix} a_{11} & a_{12} & 0 & 0 & a_{15} & 0 \\ a_{21} & a_{22} & 0 & 0 & a_{25} & 0 \\ 0 & 1 & 0 & 0 & 0 & 0 \\ v_x & l_s & v_x & 0 & 0 & 0 \\ 0 & 0 & 0 & 0 & 0 & 1 \\ a_{61} & a_{62} & 0 & 0 & a_{65} & a_{66} \end{bmatrix}, \; B = \begin{bmatrix} 0 \\ 0 \\ 0 \\ 0 \\ 0 \\ b_6 \end{bmatrix}$$

$$E(v_x) = \begin{bmatrix} e_1 & e_2 & 0 & 0 & 0 & 0 \\ 0 & 0 & 0 & -v_x & 0 & 0 \end{bmatrix}^\top$$

with

$$\begin{aligned}a_{11} &= -\frac{2(C_{f_0} + C_{r_0})}{M_v v_x}, \quad a_{12} = \frac{2(C_{r_0} l_r - C_{f_0} l_f)}{M_v v_x^2} - 1 \\ a_{15} &= \frac{2C_{f_0}}{R_s M_v v_x}, \quad a_{21} = \frac{2(C_{r0} l_r - C_{f_0} l_f)}{I_z} \\ a_{22} &= -\frac{2(C_{r_0} l_r^2 + C_{f_0} l_f^2)}{v_x I_z}, \; a_{25} = \frac{2 l_f C_{f_0}}{R_s I_z} \\ a_{61} &= \frac{2C_{f_0} g_t}{R_s J_s}, \; a_{62} = \frac{2C_{f_0} l_f g_t}{v_x R_s J_s}, \; b_6 = \frac{1}{J_s} \\ a_{65} &= \frac{-2C_{f_0} g_t}{R_s^2 J_s}, \quad a_{66} = \frac{-B_s}{J_s}, \quad e_1 = \frac{1}{M_v v_x}, \quad e_2 = \frac{l_d}{I_z}.\end{aligned}$$

Note that the nominal parts C_{f_0} and C_{r_0} of the cornering stiffness coefficients are included in $A(v_x)$, whereas the uncertain parts $\Delta_f \zeta(t)$ and $\Delta_r \zeta(t)$ are used to define $\Delta A(v_x)$ as

$$\Delta A(v_x) = H(v_x)\Delta(t) \tag{6}$$

where $\Delta(t) = \zeta(t) I \in \mathbb{R}^{6\times 6}$. The explicit expression of $H(v_x)$ can be easily obtained following the same line as [32], [33], which is omitted here for brevity.

III. Driver Activity Characterization and Dynamic Driving Assistance

This section presents the characterization of the driver activity and the dynamic driving assistance, which are crucial for shared control design.

A. Driver Activity Characterization

The driver's driving capacities strongly depend on his/her both physiological and psychological states. It has been shown that the human driver cognitive (physical and mental) workload strongly impacts on the capacity to perform certain driving tasks [34]. In addition, the authors show that there is a close relationship between the driver fatigue and a monotonous road environment. Moreover, the level of driving assistance, required by a driver, should be appropriate to his/her cognitive driving workload [5]. The relationship between the cognitive

workload and the driver task performance can be represented as the $U-$shape function [10], where the driving workload can be categorized into three types: under-load, normal-load, and over-load, as shown in Fig. 3. Most of existing shared driving control results have focused on the right-half part of the $U-$shape function [10], which is related to the *active* fatigue due to an overload workload. The left-half part of the $U-$shape is concerned with the *passive* fatigue of the driver, mainly due to his/her cognitive underload, which can also significantly decrease the driver's driving performance [35]. Indeed, an undemanding task still reduces attentional resources, which can lead to changes in driver's performance characterized by a decrease of vigilance. Many experimental researches have been performed to study various indicators to identify the passive and active fatigue of the human driver. These indicators can be classified into *direct* and *indirect* methods [36], depending on whether they come from measurements carried out on the driver for the mental workload, *e.g.*, eye blinks, head movements, etc., or on the vehicle for the physical workload, *e.g.*, steering wheel angle, steering torque, lateral position on the road, etc. A consensus has gradually emerged that a reliable diagnosis of the driver's state should be based on a combination of these two methods through a driver and driving data fusion process [37]–[39]. Hereafter, we characterize the driver's activity (DA) in function of his/her cognitive workload, *i.e.*,

- Under-load DA variable is used to represent the mental part of the driver.
- Normal-load DA variable is used to represent both the mental and physical parts of the driver.
- Over-load DA variable is used to represent the mental and physical driver state, and the risk assessment related to the driving situation.

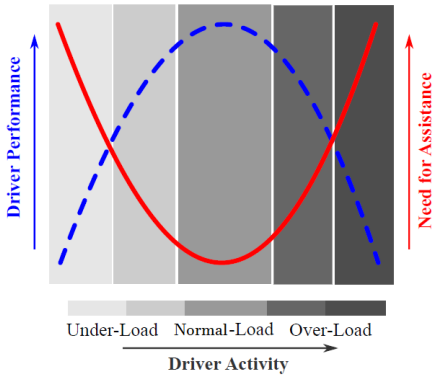

Fig. 3: Illustration of driver activity and performance, and the respective driving assistance level.

1) Under-Load DA Region: To measure the driver's drowsiness and inattention, a vision-based Continental driver monitoring system is used to evaluate the driver's gaze and eye movements, as depicted in Fig. 4. The drowsiness level, which indicates the vigilance level of the driver, can be categorized into three distinct classes, *i.e.*, watchful, drowsy and sleepy. Likewise, the inattention level indicates whether the driver focuses on the road or not.

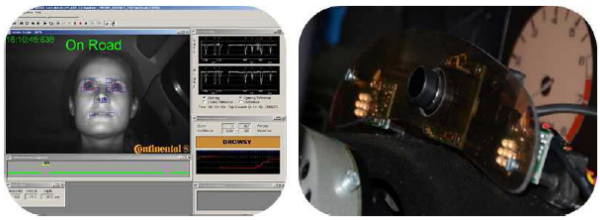

Fig. 4: Continental driver monitoring system.

To better represent the driver's activity in terms of mental workload, the driver monitoring information has been combined with the detection of the presence of the hands on the steering wheel. Then, the variable representing the DA in the under-load region is defined as

$$DA_U = 1 - \exp^{-(\sigma_1 \times \mathcal{DS} \times \mathcal{HD})^{\sigma_2}} \tag{7}$$

where $\mathcal{DS}$ is the driver state. This information can be directly obtained from the driver monitoring system. We have $0 \leq \mathcal{DS} \leq 1$, and an increased value of $\mathcal{DS}$ denotes a vigilant and attentive driver. The variable $\mathcal{HD} \in \{0, 1\}$ represents the detection of the driver's hands on the steering wheel from a hand detection sensor, *i.e.*, $\mathcal{HD} = 0$ means "hands-off", and $\mathcal{HD} = 1$ means "hands-on". The expression (7) is designed to identify situations in which the driver might be considered underloaded or in a scenario where s/he does not require assistance. This is crucial because not every instance of low torque input signifies a need for assistance. For instance, when driving straight on a clear road, minor torque fluctuations are typical and do not necessarily indicate a lack of driver awareness. Such a diving situation is not yet well represented with the DA characterization in [10].

2) Normal-Load DA Region: The physical workload is quantified by the measured torque of the driver at the steering wheel. Then, the nonlinear variable representing the DA in the normal-load region is defined as

$$DA_N = 1 - \exp^{-(\sigma_1 \times \mathcal{T}_{dN} \times \mathcal{DS} \times \mathcal{HD})^{\sigma_2}} \tag{8}$$

where the driver's physical workload is normalized by the driver's torque as $\mathcal{T}_{dN} = \left|\frac{T_d}{T_{d\,\max}}\right|$. Note that $T_{d\,\max}$ is the driver's maximum torque required for the steering task, averaged over different drivers. The expression (8) represents a typical driving scenario in which driver activity falls within an expected range. It serves as a baseline for evaluating normal driving behavior without the necessity of additional assistance.

3) Over-Load DA Region: As mentioned above, the risk assessment is also considered in the over-load DA region. We evaluate the risk of the overtaking maneuver and take it into account the arbitration process of the driving supervisor. In this context, the risk of a maneuver can be expressed as the risk of head-on and rear-end collisions with leading and trailing vehicles, respectively. To evaluate the risk, we consider the

time-inter-vehicle (TIV) metric from the ego vehicle to the adjacent vehicle as [40]

$$\begin{aligned} \mathcal{R}isk &= \frac{\mathcal{TIV}_{\max} - \mathcal{TIV}}{\mathcal{TIV}_{\max}} \\ \mathcal{TIV} &= \frac{\mathcal{D}}{v_{ego}}, \quad \mathcal{TIV}_{\max} = \frac{\mathcal{D}_{\max}}{v_{ego}} \end{aligned} \tag{9}$$

where $\mathcal{D}$ is the gap between two vehicles, and $\mathcal{D}_{\max}$ is the maximum possible distance detected by the vehicle's perception system. The variable characterizing the DA in the over-load region can be defined as

$$DA_O = 1 - \exp^{-(\sigma_1 \times \mathcal{DS} \times \mathcal{HD} \times \mathcal{R}isk)^{\sigma_2}} \tag{10}$$

The expression (10) is specifically applicable to situations in which the driver may be overloaded or confronted with demanding driving conditions. This expression helps identify when the driver may require assistance due to the increased workload, such as during emergency maneuvers.

The driver activity function plays a key role for the proposed driver-automation shared driving controller. This function determines the level of the driver's involvement in the vehicle control process with respect to the automation. The use of an *exponential* function to model the driver activity in (7), (8) and (10) avoids abrupt and sudden changes between two discrete states (0 and 1) that could lead to unstable or inappropriate system behavior. The tuning parameter σ_1 is used to represent the driver's involvement in driving tasks, while σ_2 represents the degree of influence of different indicators on the DA variable. The model parameters σ_1 and σ_2 are used as in [10]. From (7), (8) and (10), the DA variable representing the driver activity in the three working regions can be expressed as

$$DA = \frac{1}{3}\left(DA_U + DA_N + DA_O\right) \tag{11}$$

The continuity of the variable DA in (11) is ensured by the mental load indicators $\mathcal{DS}$ and $\mathcal{HD}$, which are common in the three regions. The driver activity is divided into three categories: under-load DA_U, normal-load DA_N, and over-load DA_O. The mental load indicators $\mathcal{DS}$ and $\mathcal{HD}$ are used to characterize DA_U and DA_N. Moreover, the physical indicator $\mathcal{T}_{dN}$ is used to characterize DA_N. For the over-load region, the driver activity is characterized by the mental load indicators $\mathcal{DS}$ and $\mathcal{HD}$, and the risk indicator $\mathcal{R}isk$. The overall driver activity DA is calculated in (11) as an average of the three variables DA_U, DA_N, and DA_O. Averaging these DA values creates a composite metric that accounts for various driving scenarios and mitigates potential fluctuations or outliers in individual expression outputs. Table I summarizes the availability of various DA indicators in the three workload regions.

TABLE I: DA indicators present in the three workload regions.

Driver Activity / Indicators	$\mathcal{DS}$	$\mathcal{HD}$	$\mathcal{T}_{dN}$	$\mathcal{R}isk$
DA_U	✓	✓	–	–
DA_N	✓	✓	✓	–
DA_O	✓	✓	–	✓
DA	✓	✓	✓	✓

Fig. 5 shows the DA evolution in the three workload regions for different situations according to different indicators: $\mathcal{DS}$, $\mathcal{HD}$, $\mathcal{T}_{dN}$ and $\mathcal{R}isk$.

- For $0s < t < 10s$, the driver is not available $\mathcal{DS} = 0$, then $DA = 0$.
- For $10s < t < 20s$, the driver is available $\mathcal{DS} = 1$ with the hands on the steering wheel $\mathcal{HD} = 1$. However, he/she does not apply any steering torque, *i.e.*, $\mathcal{T}_{dN} = 0$. Then, DA varies within the under-load region.
- For $21s < t < 35s$, we have $\mathcal{DS} = 1$ and $\mathcal{HD} = 1$. Moreover, the driving situation is not risky ($\mathcal{R}isk = 0$) and there is a physical activity, *i.e.*, $\mathcal{T}_{dN} \neq 0$. Then, DA varies within the normal-load region.
- For $35s < t < 50s$, we have $\mathcal{DS} = 1$ and $\mathcal{HD} = 1$. Although the driver's physical activity is non-null, but the driving situation is risky. Then, the variable DA varies within the over-load region.

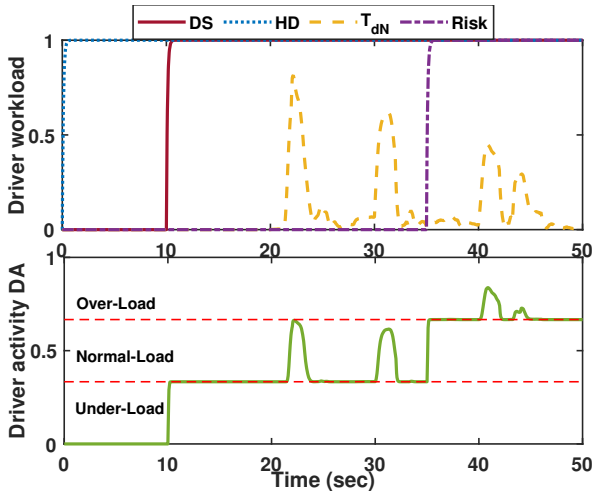

Fig. 5: Driver activity variation according to mental, physical workload indicators and risk assessment.

B. Dynamic Driving Assistance

From the DA characterization within three workload regions, the level of assistance or the need of assistance, as illustrated in Fig. 3, can be evaluated via the time-varying parameter $\rho \in [0, 1]$, defined as

$$\rho = \left(\lambda_1 \times DA_U \times (DA - \lambda_2)^2 + \lambda_3\right) + (1 - DA_U) \tag{12}$$

where λ_1, λ_2 and λ_3 are respectively given by 3.6, 0.5 and 0.1. Note from (12) that the level of assistance is conditioned by DA_U to give the control authority to the LKS if the driver is out of the driving loop. In the case where the driver is in the driving loop, the authority is shared between the LKS and the driver according to the variable DA to minimize the human-machine conflict, thus the driver's physical steering workload. When the driver's steering action leads to a risky driving situation, the variable DA is shifted to the over-load region, then the control authority is given to the LKS.

IV. LPV Shared Driving Control Design

This section presents the design of an adaptive shared controller. The driver-automation control authority is arbitrated via a dynamic cost function, which is defined taking into account the level of assistance provided by the driving supervisor. To deal with the time-varying parameters, a polytopic LPV control technique is used for the shared control design.

A. Polytopic LPV Vehicle Modeling

Note that the system matrices $A(v_x)$, $\Delta A(v_x)$ and $E(v_x)$ in (5) explicitly depend on the following speed-related terms:

$$\left\{v_x,\ \frac{1}{v_x},\ \frac{1}{v_x^2}\right\}, \quad v_{\min} \leq v_x \leq v_{\max}. \tag{13}$$

To reduce the complexity of the polytopic representation of the LPV vehicle model (5) and the induced design conservatism, we perform the following variable change and first-order Taylor approximations [3], [10]:

$$\begin{aligned} \frac{1}{v_x} &= \frac{1}{v_0} + \frac{1}{v_1}\alpha, \quad v_x \simeq v_0\left(1 - \frac{v_0}{v_1}\alpha\right) \\ \frac{1}{v_x^2} &\simeq \frac{1}{v_0^2}\left(1 + 2\frac{v_0}{v_1}\alpha\right) \end{aligned} \tag{14}$$

with $v_0 = \frac{2v_{\min}v_{\max}}{v_{\min}+v_{\max}}$ and $v_1 = \frac{2v_{\min}v_{\max}}{v_{\min}-v_{\max}}$. Note that the new time-varying parameter $\alpha \in [-1, 1]$ can be used to describe the variation of v_x, *i.e.*, $v_x = v_{\min}$ for $\alpha = \alpha_{\min} = -1$, and $v_x = v_{\max}$ for $\alpha = \alpha_{\max} = 1$. Replacing (14) into (5), we obtain a vehicle model, whose state-space matrices linearly and solely depend on α. Then, using the sector nonlinearity approach [41, Chapter 2], we can derive the following polytopic LPV representation of model (5):

$$\Sigma_\alpha:\ \dot{x} = \sum_{i=1}^{2} h_i(\alpha)((A_i + \Delta A_i)x + E_i d) + Bu \tag{15}$$

where the state-space matrices of the two linear submodels are given by

$$\begin{aligned} \Sigma_{\alpha 1}:&\quad A(\alpha_{\min}),\ B,\ E(\alpha_{\min}) \\ \Sigma_{\alpha 2}:&\quad A(\alpha_{\max}),\ B,\ E(\alpha_{\max}). \end{aligned}$$

It follows from (6) that ΔA_i can be represented as

$$\Delta A_i = H_i \Delta(t), \quad i = 1, 2 \tag{16}$$

with $\Delta(t)^\top \Delta(t) \leq I$. Furthermore, the membership functions of the polytopic LPV model (15) are defined as

$$h_1(\alpha) = \frac{1-\alpha}{2}, \quad h_2(\alpha) = 1 - h_1(\alpha). \tag{17}$$

B. LPV Shared Control Design

To take into account the lane-keeping performance, we define the performance output of system (15) as

$$z = Cx = \begin{bmatrix}\beta & r & \psi_L & y_L & \dot{\delta}_d\end{bmatrix}. \tag{18}$$

For shared control purposes, the following cost function is defined to take into account the dynamic driving assistance, represented by the time-varying parameter ρ in (12):

$$\mathscr{J}(\rho) = \int_0^\infty \left(z^\top(\tau)\rho Q z(\tau) + u^\top(\tau) R u(\tau)\right) d\tau \tag{19}$$

where $Q = W^\top W \succ 0$ and $R \succ 0$ are the weighting matrices. Since $\rho \in [0, 1]$, we can perform the decomposition

$$\rho Q = \left(\sum_{j=1}^{2} g_j(\rho) W_j\right)^\top \left(\sum_{j=1}^{2} g_j(\rho) W_j\right) \tag{20}$$

with $g_1(\rho) = \sqrt{\rho}$, $g_2(\rho) = 1 - g_1(\rho)$, $W_1 = W$ and $W_2 = 0$.

Remark 1. Inspired by the well-known principle of an linear quadratic regulator (LQR), we can see in (19) that when the control authority is entirely entrusted to the LKS, *i.e.*, $\rho = 1$, the control action T_c is designed to achieve the best lane keeping performance by mainly penalizing the lane-keeping related term $z^\top(\tau)\rho Q z(\tau)$. Conversely, when the control authority is entirely allocated to the human driver, *i.e.*, $\rho = 0$, a minimized control action T_c is designed to minimize $\mathscr{J}(\rho)$ by penalizing the control effort term $u^\top(\tau) R u(\tau)$. Hence, integrating the time-varying parameter ρ into the cost function $\mathscr{J}(\rho)$ allows to adaptively balance the control authority between the human driver and the LKS in function of the driving situation and the specific need of assistance from the driver without a direct weighting of the control input as in most of existing related works on driver-automation shared control [16]. This can contribute to improving driving safety and comfort while avoiding human-machine conflicts.

We consider the following LPV control law for system (15):

$$u = \sum_{i=1}^{2}\sum_{j=1}^{2} h_i(\alpha) g_j(\rho) K_{ij} x \tag{21}$$

where the control gains with of appropriate dimensions K_{ij}, for $i, j \in \{1, 2\}$, are to be determined. Then, the closed-loop system can be defined from (15) and (21) as

$$\Sigma_{\alpha\rho}:\ \dot{x} = \sum_{i=1}^{2}\sum_{j=1}^{2} h_i(\alpha) g_j(\rho)((\hat{A}_i + BK_{ij})x + E_i d) \tag{22}$$

with $\hat{A}_i = A_i + \Delta A_i$. For control synthesis, we consider the Lyapunov function candidate as

$$\mathcal{V}(x) = x^\top P x \tag{23}$$

with $P \succ 0$. The following theorem provides sufficient LMI-based conditions to design the LPV controller (21).

Theorem 1. If there exist a positive definite matrix X, matrices N_{ij}, for $i, j \in \{1, 2\}$, of appropriate dimensions, positive scalars γ and ε such that

$$\begin{bmatrix} \Gamma_{ij} & \varepsilon\Xi_i & \Lambda^\top \\ * & -\varepsilon I & 0 \\ * & * & -\varepsilon I \end{bmatrix} \prec 0, \quad i, j \in \{1, 2\} \tag{24}$$

with

$$\Gamma_{ij} = \begin{bmatrix} \mathrm{He}(A_i X + BN_{ij}) & E_i & XC^\top W_j^\top & N_{ij}^\top \\ * & -\gamma I & 0 & 0 \\ * & * & -I & 0 \\ * & * & * & -R^{-1} \end{bmatrix}$$

$$\Xi_i = \begin{bmatrix} H_i^\top & 0 & 0 & 0 \end{bmatrix}^\top, \quad \Lambda = \begin{bmatrix} X & 0 & 0 & 0 \end{bmatrix}.$$

Then, the LPV controller (21) stabilizes the vehicle system (15), and guarantees an upper-bound for the cost function (19) under zero-initial condition as

$$\mathscr{J}(\rho) < \gamma \|d\|_2^2. \tag{25}$$

Furthermore, the feedback control gains can be computed as

$$K_{ij} = N_{ij} X^{-1}, \quad i,j \in \{1,2\}. \tag{26}$$

Proof. Multiplying (24) with $h_i(\alpha) g_j(\rho) \geq 0$, and summing up for $i,j = 1,2$, we can obtain

$$\begin{bmatrix} \Gamma_{\alpha\rho} & \varepsilon \Xi_\alpha & \Lambda^\top \\ * & -\varepsilon I & 0 \\ * & * & -\varepsilon I \end{bmatrix} \prec 0 \tag{27}$$

with $\Gamma_{\alpha\rho} = \sum_{i=1}^{2}\sum_{j=1}^{2} h_i(\alpha) g_j(\rho) \Gamma_{ij}$ and $\Xi_\alpha = \sum_{i=1}^{2} h_i(\alpha) \Xi_i$. Applying successively two times the Schur complement lemma [42], we can show that inequality (27) is equivalent to

$$\Gamma_{\alpha\rho} + \varepsilon \Xi_\alpha \Xi_\alpha^\top + \varepsilon^{-1} \Lambda^\top \Lambda \prec 0. \tag{28}$$

Using the following matrix property [42]

$$\Xi_\alpha \Delta(t) \Lambda + \Lambda^\top \Delta(t) \Xi_\alpha^\top \prec \varepsilon \Xi_\alpha \Xi_\alpha^\top + \varepsilon^{-1} \Lambda^\top \Lambda$$

condition (28) implies that

$$\Gamma_{\alpha\rho} + \Xi_\alpha \Delta(t) \Lambda + \Lambda^\top \Delta(t) \Xi_\alpha^\top \prec 0. \tag{29}$$

Using expression (16), inequality (29) can be rewritten as

$$\begin{bmatrix} \Sigma_{\alpha\rho} & E_i & X C^\top W_j^\top & N_{ij}^\top \\ * & -\gamma I & 0 & 0 \\ * & * & -I & 0 \\ * & * & * & -R^{-1} \end{bmatrix} \prec 0 \tag{30}$$

with $\Sigma_{\alpha\rho} = \sum_{i=1}^{2}\sum_{j=1}^{2} h_i(\alpha) g_j(\rho) \mathrm{He}(\hat{A}_i X + B N_{\alpha\rho})$. Applying again the Schur complement lemma, it follows that inequality (30) is equivalent to

$$\begin{bmatrix} \Sigma_{\alpha\rho} + N_{\alpha\rho}^\top R N_{\alpha\rho} + X C^\top \rho Q C X & E_i \\ * & -\gamma I \end{bmatrix} \prec 0. \tag{31}$$

Let us denote $P = X^{-1}$ and $N_{\alpha\rho} = K_{\alpha\rho} X$. Pre- and post-multiplying (31) with $\mathrm{diag}(P, I)$, it follows that

$$\begin{bmatrix} \Pi_{\alpha\rho} + K_{\alpha\rho}^\top R K_{\alpha\rho} + C^\top \rho Q C & P E_\alpha \\ * & -\gamma I \end{bmatrix} \prec 0 \tag{32}$$

where $\Pi_{\alpha\rho} = \mathrm{He}(P(\hat{A}_\alpha + B K_{\alpha\rho}))$. Pre- and post-multiplying (32) with $\begin{bmatrix} x^\top & d^\top \end{bmatrix}^\top$ and its transpose, we can obtain the following condition after some algebraic manipulations:

$$\dot{\mathcal{V}}(x) + z^\top \rho Q z + u^\top R u < \gamma d^\top d \tag{33}$$

where $\dot{\mathcal{V}}(x)$ is the time-derivative of the Lyapunov function (23) along the trajectory of the closed-loop system (15). From (33), we distinguish the two following cases.

• **Case 1.** If $d(t) = 0$, for $\forall t \geq 0$. Then, it follows from (33) that $\dot{\mathcal{V}}(x) < 0$, for $\forall x \neq 0$. Hence, the closed-loop-system (15) is globally exponentially stable.

• **Case 2.** If $d(t) \neq 0$, for $\forall t \geq 0$. Then, integrating both sides of (33) from 0 to ∞, it leads to

$$\mathcal{V}(\infty) - \mathcal{V}(0) + \mathscr{J}(\rho) < \gamma \int_0^\infty d^\top(t) d(t). \tag{34}$$

Since $\mathcal{V}(\infty) > 0$, under zero initial condition, *i.e.*, $\mathcal{V}(0) = 0$, it is clear that (34) implies inequality (25). Note also from (25) that the adaptive cost function $\mathscr{J}(\rho)$ can be minimized by minimizing γ. Then, the proof can be concluded. □

Remark 2. The control design conditions in Theorem 1 are expressed in terms of LMIs, which can be effectively solved with YALMIP toolbox and SeDuMi solver [43].

V. Experimental Validations

This section provides illustrative results to demonstrate the performance of the proposed shared controller in terms of conflict reduction and lane-keeping. All the experiments are performed with the SHERPA dynamic car driving simulator, depicted in Fig. 6, under highway driving conditions. The values of the control parameters and the vehicle parameters used in this paper are shown in Table II. Solving the LMI design conditions in Theorem 1, the following control feedback gains can be obtained for real-time experiments:

$$\begin{aligned} K_{11} &= -\begin{bmatrix} 105.44 & 8.19 & 131.62 & 3.38 & 8.67 & 0.03 \end{bmatrix} \\ K_{12} &= \begin{bmatrix} 9.29 & 0.79 & 12.53 & 0.32 & 0.83 & 0.01 \end{bmatrix} \\ K_{21} &= -\begin{bmatrix} 110.43 & 8.35 & 137.59 & 3.54 & 9.06 & 0.03 \end{bmatrix} \\ K_{22} &= \begin{bmatrix} 9.98 & 0.81 & 13.65 & 0.34 & 0.90 & 0.01 \end{bmatrix}. \end{aligned}$$

Fig. 6: SHERPA dynamic driving simulator.

TABLE II: Control design and vehicle parameters.

Parameter	Value	Unit	Parameter	Value	Unit
l_f	1.3	m	J_s	0.05	$kg.m^2$
l_r	1.6	m	C_{f_0}	57000	N/rad
l_w	0.4	m	C_{r_0}	59000	N/rad
l_p	5	m	R_s	16	–
B_s	5.73	–	v_x	[8,30]	m/s
R_s	0.9	–	g_t	0.13	m
I_z	2800	$kg.m^2$	M_v	2024	kg
W	diag(9,9,5,8,5)	–	ρ	[0,1]	–

A. Robustness Control Performance

We perform three tests to evaluate the robustness performance of the proposed shared controller in self-driving mode with respect to the time-varying vehicle speed, external disturbances, and tires stiffness uncertainties.

First, the lane keeping performance results obtained with a time-varying vehicle speed profile are presented in Fig. 7. With the lane width of $3.5m$, we can see that the LKS ensures a good lane keeping performance, where the maximum lateral and heading errors are $|y_L|_{max} = 0.6m$ and $|\psi_L|_{max} = 0.37deg$, respectively.

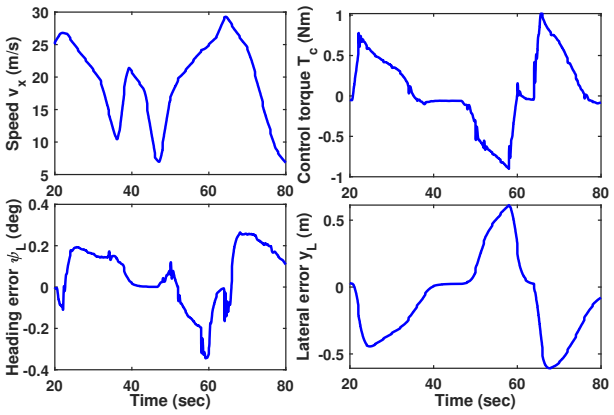

Fig. 7: Lane keeping performance with a time-varying vehicle speed profile.

Second, to show the control robustness against external disturbances, an automatic driving test is performed with a constant speed of $v_x = 22m/s$ and a strong lateral wind force with a magnitude of $1000N$. Observe in Fig. 8 that the wind disturbance effect can be effectively attenuated since the maximum lateral and heading errors still remain small during the test, *i.e.*, $|y_L|_{max} = 0.98m$ and $|\psi_L|_{max} = 0.41deg$, respectively.

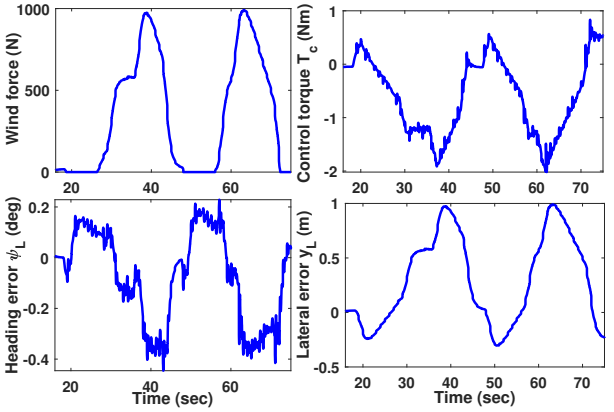

Fig. 8: Lane keeping performance under a strong crosswind disturbance scenario.

Third, to verify the control robustness with respect to the tires stiffness uncertainties, we use random parametric variations in the vehicle parameters to consider uncertain values of C_f and C_r. For comparison purposes, we evaluate the lane keeping performance obtained with two controllers: Controller C1 proposed in [31] without considering the stiffness uncertainties, and Controller C2 proposed in this paper. The comparison results are summarized in Table III. We can see that the amplitudes of the maximum lateral deviation and heading errors are more notable for Controller C1 than Controller C2. Indeed, for 20% of parameter variation, we can note $|y_L|_{\max} = 0.537m$, $|\psi_L|_{\max} = 0.388deg$ for Controller C2, and $|y_L|_{\max} = 0.647m$, $|\psi_L|_{\max} = 0.422deg$ for Controller C1. In addition, it can be seen that the steering effort provided by Controller C1 is smaller than that of Controller C2, which confirms the effectiveness of the proposed controller in handling parametric uncertainties.

TABLE III: Lane keeping control performance with respect to parametric uncertainties.

Uncertainty	Controller	$\lvert y_L\rvert_{\max}$	$\lvert\psi_L\rvert_{\max}$	$\lvert T_a\rvert_{\max}$
5%	C1	0.628	0.391	1.245
	C2	0.509	0.377	1.074
10%	C1	0.641	0.404	1.392
	C2	0.516	0.382	1.152
20%	C1	0.674	0.422	1.446
	C2	0.537	0.388	1.211

B. Adaptive Shared Control with Risk Assessment

This test presents an example on how the proposed shared controller can ensure a safe driving in a risky situation. To this end, we consider an overtaking scenario at a constant vehicle speed, where the human driver jointly controls the vehicle with the LKS automation, and is instructed to overtake two other vehicles on the highway. The first overtaking is safe, while the second one is risky due to the presence of another car on the left lane, as depicted in Fig. 9. The results of this test scenario are presented in Fig. 10.

- During the first overtaking (at $t = 28s$), we can see that the human driver can easily executes the driving task. The level of assistance decreases when the DA is in the normal-load region, *i.e.*, the driving authority is given to the driver.
- During the second overtaking (at $t = 60s$), the driver is guided by the shared controller to stay within the current lane ($y_L < 1m$) because the driving situation is risky. Also, the DA shifts to the over-load region, which means that the driver needs to be assisted to avoid a crash with the adjacent vehicle. Therefore, the assistance level increases to 1 to give the authority to the LKS automation.
- When the adjacent vehicle moves forward and the situation becomes safe, the driver performs the third overtaking (at $t = 65s$). We can see that he can easily pass the second vehicle, and the level of assistance decreases to allow the driver to control the vehicle since the DA decreases to the normal-load region.

C. User-Test Experiments

Hereafter, the vehicle control results obtained with user-test experiments are presented. Both objective and subjective

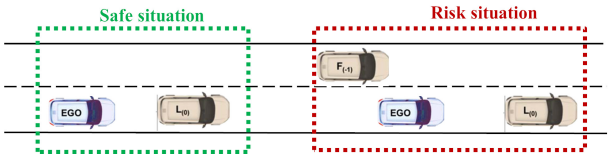

Fig. 9: Risky and non-risky lane change scenarios.

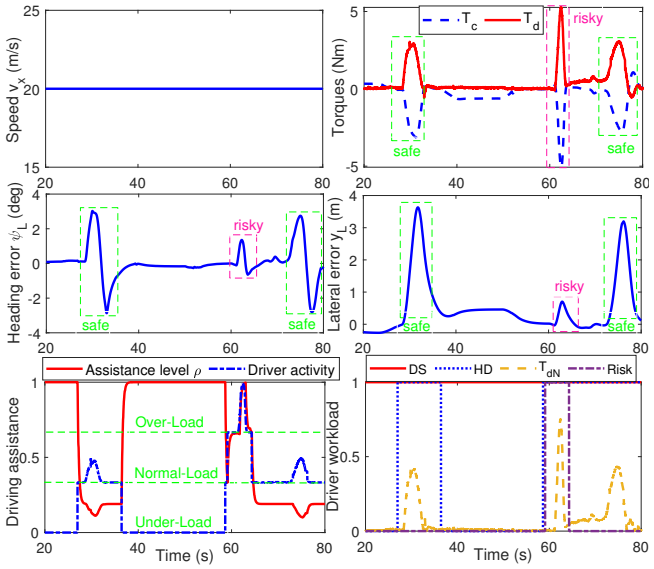

Fig. 10: Shared control performance for risky and non-risky lane change scenarios.

evaluations are made for an obstacle avoidance scenario to compare the proposed shared controller with the one in [10], where there is no adaptive cost function.

Six participants took part in these experiments (4 males and 2 females). The average age is 34 ± 9 years, and an average annual mileage of $8500km$. A short obstacle avoidance scenario was considered. The experiment took place on a straight two-lane road that extends for $4km$. With the instruction to stay in the lane, the drivers were required to avoid several stopped obstacles. The participants were asked to change the lanes to avoid possible collisions, while driving at a fixed speed of $70km/h$. This speed allows to easily compare the driving behaviors between different participants by avoiding inter-individual differences in the choice of vehicle speed, and by assuming also that obstacles are not perceived by the system. With the same scenario, the participants drove with three control strategies:

- $Manual$: manual control strategy
- LKS_{WOA}: lane keeping control strategy with the shared controller in [10]
- LKS_{WA}: proposed adaptive shared control strategy.

Questionnaires were provided after each test phase to collect a subjective assessment of the driving experience. The data analysis is divided into two parts.

1) Objective Evaluation: This evaluation is carried out by using indicators to evaluate the human-machine interaction and the shared control quality. The four following metrics are analyzed for this study as in [20].

- Driver steering effort during the experimental period T_{ex}

$$StD = \int_0^{T_{ex}} T_d^2(\tau) d\tau \tag{35}$$

- Controller steering effort during the experimental period

$$StC = \int_0^{T_{ex}} T_a^2(\tau) d\tau \tag{36}$$

- Driver-automation conflict during the experimental period

$$Conflict = \int_0^{T_{ex}} |T_a(\tau) - T_d(\tau)| \, d\tau \tag{37}$$

- Steering workload SW generated when the driver interacts with the automation to jointly perform the driving

$$SW = \int_0^{T_{ex}} \left| T_a(\tau) \cdot T_d(\tau) \cdot \dot{\delta}_d(\tau) \right| d\tau \tag{38}$$

As shown in Fig. 11, using the LKS_{WOA} strategy, the effort required to steer the vehicle and avoid obstacles is very high when the system is not cooperating when compared to the manual control strategy. However, the LKS_{WA} strategy leads to a driver's driving effort of the same order as under the manual control condition. It is also clear from Fig. 11 that using the LKS_{WA} strategy the LKS system significantly reduces its effort and resistance to the driver compared to the LKS_{WOA} control condition. The quantitative results strongly demonstrate that the proposed shared control method is highly effective in mitigating the driver's effort and the driver-automation conflict.

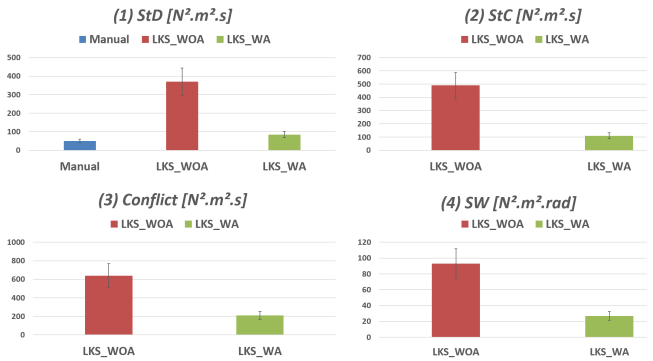

Fig. 11: Objective evaluation of different shared control strategies under an obstacle avoidance scenario.

2) Subjective Evaluation: The questionnaires provided to the participants allow for an analysis of subjective data. This consists of five metrics, including driving comfort, feeling of control and safety, ease of avoiding obstacles, and global evaluation of the overall driving performance for each test phase. The first four subjective metrics are reported on a scale

of 0 to 100 (worst to best). The fifth metric is a simple choice of one of the three possibilities: *Good*, *Medium* or *Bad*. As reported in Fig. 12, compared to the other two control strategies, the LKS_{WOA} strategy allows achieving the lowest level for the four subjective metrics: *Control*, *Comfort*, *Easiness* and *Safety*. We can see clearly via these four metrics that the feeling of control, the comfort, the ease of obstacle avoidance and the feeling of security and trust in the LKS system are rated worse with the LKS_{WOA} strategy, whereas the LKS_{WA} strategy results in an equivalent or slightly lower feeling than the *Manual* strategy. Finally, the subjective evaluation of the overall driving performance during the test scenario with the different conditions is shown in Fig. 13. As expected, the perceived driving performance during the obstacle avoidance is the worst with the LKS_{WOA} strategy.

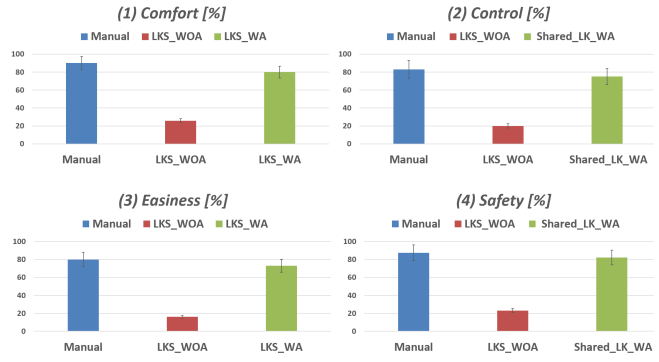

Fig. 12: Subjective evaluation of different shared control strategies under an obstacle avoidance scenario.

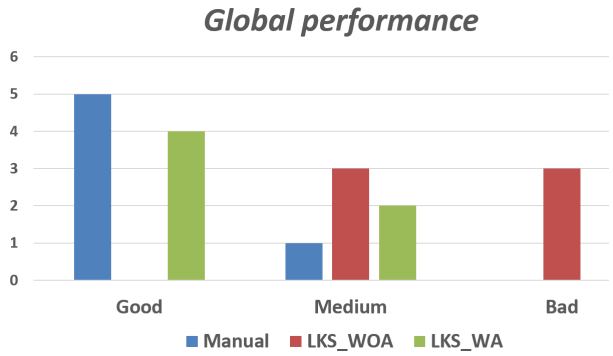

Fig. 13: Global driving performance of different shared control strategies under an obstacle avoidance scenario.

VI. Conclusions and Future Works

An LPV method has been proposed for shared driving control while managing the authority between the human driver and the LKS system. Based on an adaptive cost function for the control design, the level of assistance is dynamically adjusted according to the driving conditions as well as the availability and the driving activity of the driver in real-time. The LPV control design takes into account the time-varying nature of the vehicle speed and the driving assistance level, as well as the uncertainties in the lateral tires forces. Based on Lyapunov stability theory, the control design conditions are expressed in terms of LMI constraints, where the adaptive cost function can be minimized under the disturbance effects. User-test experiments are performed with the SHERPA dynamic car simulator. The experimental results show the effectiveness of the proposed shared control method over related existing works in terms of control robustness, and especially driver acceptability with a minimized level of driver-automation conflict driver effort. For future works, a dynamic impedance driver model can be integrated into the shared control scheme to further personalize the cooperative LKS functionalities.

References

[1] S. Kato, E. Takeuchi, Y. Ishiguro, Y. Ninomiya, K. Takeda, and T. Hamada, "An open approach to autonomous vehicles," *IEEE Micro*, vol. 35, no. 6, pp. 60–68, 2015.

[2] M. Hasenjäger, M. Heckmann, and H. Wersing, "A survey of personalization for advanced driver assistance systems," *IEEE Trans. Intell. Veh.*, vol. 5, no. 2, pp. 335–344, 2019.

[3] P. Li, Y. Wang, and H. Zhang, "Polytopic LPV approaches for intelligent automotive systems: State of the art and future challenges," *Mech. Syst. Signal Process.*, vol. 161, p. 107931, 2021.

[4] X. Zhou, H. Shen, Z. Wang, H. Ahn, and J. Wang, "Driver-centric lane-keeping assistance system design: A noncertainty-equivalent neuro-adaptive control approach," *IEEE/ASME Trans. Mechatron.*, pp. 1–12, 2023, DOI: 10.1109/TMECH.2023.3236245.

[5] C. Sentouh, A.-T. Nguyen, A. Benloucif, and J.-C. Popieul, "Driver-automation cooperation oriented approach for shared control of lane keeping assist systems," *IEEE Trans. Control Syst. Technol.*, vol. 27, no. 5, pp. 1962–1978, 2018.

[6] Y. Xing, C. Lv, D. Cao, and P. Hang, "Toward human-vehicle collaboration: Review and perspectives on human-centered collaborative automated driving," *Transp. Res. Part C Emerg.*, vol. 128, p. 1199, 2021.

[7] T. Saito, T. Wada, and K. Sonoda, "Control authority transfer method for automated-to-manual driving via a shared authority mode," *IEEE Trans. Intell. Veh.*, vol. 3, no. 2, pp. 198–207, 2018.

[8] Z. Zhang, C. Wang, W. Zhao, C. Xu, and G. Chen, "Driving authority allocation strategy based on driving authority real-time allocation domain," *IEEE Trans. Intell. Transp. Syst.*, vol. 3, no. 7, pp. 28–43, 2022.

[9] B. Pano, P. Chevrel, F. Claveau, C. Sentouh, and F. Mars, "Obstacle avoidance in highly automated cars: can progressive haptic shared control make it safer and smoother?" *IEEE Trans. Hum.-Mach. Syst.*, vol. 52, no. 4, pp. 547–556, 2022.

[10] A.-T. Nguyen, C. Sentouh, and J.-C. Popieul, "Driver-automation cooperative approach for shared steering control under multiple system constraints: Design and experiments," *IEEE Trans. Indus. Electron.*, vol. 64, no. 5, pp. 3819–3830, 2016.

[11] M. Flad, L. Fröhlich, and S. Hohmann, "Cooperative shared control driver assistance systems based on motion primitives and differential games," *IEEE Trans. Hum.-Mach. Syst.*, vol. 47, no. 5, pp. 11–22, 2017.

[12] M. Li, H. Cao, G. Li, S. Zhao, X. Song, Y. Chen, and D. Cao, "A two-layer potential-field-driven model predictive shared control towards driver-automation cooperation," *IEEE Trans. Intell. Transp. Syst.*, vol. 23, no. 5, pp. 4415–4431, 2022.

[13] T. Wada, K. Sonoda, and S. Tada, "Simultaneous achievement of supporting human drivers and improving driving skills by shared and cooperative control," *IFAC-PapersOnLine*, vol. 4, no. 1, pp. 90–95, 2016.

[14] Z. Wang, R. Zheng, T. Kaizuka, K. Shimono, and K. Nakano, "The effect of a haptic guidance steering system on fatigue-related driver behavior," *IEEE Trans. Hum.-Mach. Syst.*, vol. 47, no. 5, pp. 741–748, 2017.

[15] R. Luo, Y. Weng, Y. Wang, P. Jayakumar, M. Brudnak, V. Paul, V. Desaraju, J. Stein, T. Ersal, and J. Yang, "A workload adaptive haptic shared control scheme for semi-autonomous driving," *Accid. Anal. Prev.*, vol. 152, p. 105968, 2021.

[16] M. Marcano, S. Díaz, J. Pérez, and E. Irigoyen, "A review of shared control for automated vehicles: Theory and applications," *IEEE Trans. Hum.-Mach. Syst.*, vol. 50, no. 6, pp. 475–491, 2020.

[17] S. Ansari, F. Naghdy, and H. Du, "Human-machine shared driving: Challenges and future directions," *IEEE Trans. Intell. Veh.*, vol. 7, no. 3, pp. 499–519, 2022.

[18] A. Benloucif, A.-T. Nguyen, C. Sentouh, and J.-C. Popieul, "Cooperative trajectory planning for haptic shared control between driver and automation in highway driving," *IEEE Trans. Indus. Electron.*, vol. 66, no. 12, pp. 9846–9857, 2019.
[19] M. Huang, W. Gao, Y. Wang, and Z.-P. Jiang, "Data-driven shared steering control of semi-autonomous vehicles," *IEEE Trans. Hum.-Mach. Syst.*, vol. 49, no. 4, pp. 350–361, 2019.
[20] M. R. Oudainia, C. Sentouh, A.-T. Nguyen, and J.-C. Popieul, "Online driver model parameter identification using the Lyapunov approach based shared control," *Front. Control Eng.*, vol. 3, 2022.
[21] X. Li, Y. Wang, C. Su, X. Gong, J. Huang, and D. Yang, "Adaptive authority allocation approach for shared steering control system," *IEEE Trans. Intell. Transp. Syst.*, vol. 23, no. 10, pp. 19 428–19 439, 2022.
[22] J. Wu, J. Zhang, Y. Tian, and L. Li, "A novel adaptive steering torque control approach for human–machine cooperation autonomous vehicles," *IEEE Trans. Transp. Electrification*, vol. 7, no. 4, pp. 2516–2529, 2021.
[23] H. Deng, Y. Zhao, S. Feng, Q. Wang, and F. Lin, "Shared control for intelligent vehicle based on handling inverse dynamics and driving intention," *IEEE Trans. Veh. Technol.*, vol. 71, no. 3, pp. 706–720, 2022.
[24] C. Huang, C. Lv, P. Hang, Z. Hu, and Y. Xing, "Human–machine adaptive shared control for safe driving under automation degradation," *IEEE Intell. Transp. Syst. Mag.*, vol. 14, no. 2, pp. 53–66, 2021.
[25] J. Liu, Q. Dai, H. Guo, J. Guo, and H. Chen, "Human-oriented online driving authority optimization for driver-automation shared steering control," *IEEE Trans. Intell. Veh.*, vol. 7, no. 4, pp. 863–872, 2022.
[26] R. Li, Y. Li, S. E. Li, C. Zhang, E. Burdet, and B. Cheng, "Indirect shared control for cooperative driving between driver and automation in steer-by-wire vehicles," *IEEE Trans. Intell. Transp. Syst.*, vol. 22, no. 12, pp. 7826–7836, 2020.
[27] W. Li, Q. Li, S. E. Li, R. Li, Y. Ren, and W. Wang, "Indirect shared control through non-zero sum differential game for cooperative automated driving," *IEEE Trans. Intell. Transp. Syst.*, vol. 23, no. 9, pp. 15 980–15 992, 2022.
[28] X. Zhao, Z. Yin, Z. He, L. Nie, K. Li, Y. Kuang, and C. Lei, "Indirect shared control strategy for human-machine cooperative driving on hazardous curvy roads," *IEEE Trans. Intell. Veh.*, vol. 8, no. 3, pp. 2257–2270, 2023.
[29] Y. Lu, J. Liang, G. Yin, L. Xu, J. Wu, J. Feng, and F. Wang, "A shared control design for steering assistance system considering driver behaviors," *IEEE Trans. Intell. Veh.*, vol. 8, no. 1, pp. 900–911, 2023.
[30] J. Han, J. Zhao, B. Zhu, and D. Song, "Adaptive steering torque coupling framework considering conflict resolution for human-machine shared driving," *IEEE Trans. Intell. Transp. Syst.*, vol. 23, no. 8, pp. 10 983–10 995, 2022.
[31] M. R. Oudainia, C. Sentouh, A.-T. Nguyen, and J.-C. Popieul, "Dynamic conflict mitigation for cooperative driving control of intelligent vehicles," in *IEEE Intell. Veh. Symp. (IV)*, 2022, pp. 1445–1452.
[32] A.-T. Nguyen, J. Rath, T. Guerra, R. Palhares, and H. Zhang, "Robust set-invariance based fuzzy output tracking control for vehicle autonomous driving under uncertain lateral forces and steering constraints," *IEEE Trans. Intell. Transp. Syst.*, vol. 22, no. 9, pp. 5849–5860, 2021.
[33] C. Hu, H. Jing, R. Wang, F. Yan, and M. Chadli, "Robust $\mathscr{H}_\infty$ output-feedback control for path following of autonomous ground vehicles," *Mech. Syst. Signal Process.*, vol. 70, pp. 414–427, 2016.
[34] X. Zhao and J. Rong, *The Relationship between Driver Fatigue and Monotonous Road Environment*. Paris: Atlantis Press, 2013, pp. 19–36. [Online]. Available: https://doi.org/10.2991/978-94-91216-80-0_2
[35] T. McWilliams and N. Ward, "Underload on the road: Measuring vigilance decrements during partially automated driving," *Front. Psychol.*, vol. 12, 2021.
[36] S. Boverie and A. Giralt, "Driver vigilance diagnostic based on eyelid movement observation," *IFAC Proc. Vol.*, vol. 41, no. 2, pp. 12 831–12 836, 2008.
[37] T. Liu, Y. Yang, G.-B. Huang, Y. K. Yeo, and Z. Lin, "Driver distraction detection using semi-supervised machine learning," *IEEE Trans. Intell. Transp. Syst.*, vol. 17, no. 4, pp. 1108–1120, 2016.
[38] G. Li, W. Yan, S. Li, X. Qu, W. Chu, and D. Cao, "A temporal–spatial deep learning approach for driver distraction detection based on EEG signals," *IEEE Trans. Autom. Sci. Eng.*, vol. 19, no. 4, pp. 65–77, 2021.
[39] X. Wang, R. Xu, S. Zhang, Y. Zhuang, and Y. Wang, "Driver distraction detection based on vehicle dynamics using naturalistic driving data," *Transp. Res. C: Emerg. Technol.*, vol. 136, p. 103561, 2022.
[40] M. R. Oudainia, C. Sentouh, A.-T. Nguyen, and J.-C. Popieul, "Personalized decision making and lateral path planning for intelligent vehicles in lane change scenarios," in *IEEE 25th Inter. Conf. Intell. Transp. Syst. (ITSC)*, 2022, pp. 4302–4307.
[41] K. Tanaka and H. Wang, *Fuzzy Control Systems Design and Analysis: a Linear Matrix Inequality Approach*. John Wiley & Sons, 2004.
[42] S. Boyd, L. El Ghaoui, E. Feron, and V. Balakrishnan, *Linear matrix inequalities in system and control theory*. SIAM, 1994.
[43] J. Löfberg, "YALMIP: A toolbox for modeling and optimization in Matlab," in *Proc. IEEE Int. Symp. CACSD*, Taipei, 2004, pp. 284–289.

Mohamed Radjeb Oudainia received the M.Sc. degree in automatic control from the Université Polytechnique Hauts-de-France (UPHF), Valenciennes, France, and the degree of engineer in automatic control from ESSA-Tlemcen, Algeria, both in 2020. He is currently a PhD student at the LAMIH UMR CNRS 8201 laboratory, UPHF, France. His research interests include automotive control, cooperation in intelligent transportation systems and shared control for assistance systems.

Chouki Sentouh received the M.Sc. degree in automatic control from the University of Versailles, France, in 2003 and the PhD degree in automatic control from the University of Evry, France, in 2007. He is an Associate Professor at the Université Polytechnique Hauts-de-France, laboratory LAMIH UMR CNRS 8201, France. His research fields include robust control and observation applied to automotive control, driver assistance systems, human driver modeling and cooperation in intelligent transportation systems.

Anh-Tu Nguyen received the Diplôme d'Ingénieur and the M.Sc. degree in automatic control from Grenoble-INP, France, in 2009, and the PhD degree in automatic control from the University of Valenciennes, France, in 2013. He is an Associate Professor at the Université Polytechnique Hauts-de-France, and a researcher at the laboratory LAMIH UMR CNRS 8201, Valenciennes, France. His research interests include robust control and observation, human-machine shared control with strong emphasis on mechatronics applications.

Jean-Christophe Popieul is Professor in Automatic Control at "Université Polytechnique Hauts-de-France" in LAMIH-UMR CNRS 8201. Specialized in Human Centered Automation, he participated in many collaborative projects dealing with ADASs. He is currently working on control sharing for driving automation and is the coordinator of the RITMEA project with 350 researchers involved and the ANR CoCoVeIA project.